Exposing the interplay between enzyme turnover, protein dynamics and the membrane environment in monoamine oxidase B

Hannah B. L. Jones[†], Rory M. Crean[#†], Anna Mullen[§], Emanuele G. Kendrick[†], Steven D Bull[Δ], Stephen A. Wells[‡], David R. Carbery[Δ], Fraser MacMillan[§], Marc W. Van der Kamp*[%], Christopher R. Pudney*[†].

[†]Department of Biology and Biochemistry, [Δ]Department of Chemistry, [‡] Department of Chemical Engineering and [#] Doctoral Training Centre in Sustainable Chemical Technologies, University of Bath, Bath BA2 7AY, United Kingdom.

[%]School of Biochemistry, University of Bristol, Biomedical Sciences building, University Walk, Bristol BS8 1TD, United Kingdom.

[§]School of Chemistry, University of East Anglia, Norwich Research Park, Norwich NR4 7TJ, United Kingdom.

ABSTRACT: There is an increasing realization that structure-based drug design may show improved success rates by understanding the ensemble of conformations and sub-states accessible to an enzyme and how the environment affects this ensemble. Human monoamine oxidase B (MAO-B) catalyzes the oxidation of amines and is inhibited for the treatment of both Parkinson's disease and depression. Despite its clinical importance, its catalytic mechanism remains unclear and new routes to drugging this target would be valuable and relevant. Evidence of a radical in either the transition state or resting state of MAO-B is present throughout the literature, and is suggested to be a flavin semiquinone, a tyrosyl radical or both. Here we see evidence of a resting state flavin semiquinone, via absorption redox studies and electron paramagnetic resonance, suggesting that the anionic semiquinone is biologically relevant. Based on enzyme kinetic studies, enzyme variants and molecular dynamics simulations we find evidence for the crucial importance of the membrane environment in mediating the activity of MAO-B and that this mediation is related to effects on the protein dynamics of MAO-B. Further, our MD simulations identify a hitherto undescribed entrance for substrate binding, membrane modulated substrate access, and indications for half-site reactivity: only one active site is accessible to binding at a time. Our study therefore combines both experimental and computational evidence to illustrate the subtle interplay between enzyme activity, protein dynamics and the immediate membrane environment. Understanding key biomedical enzymes to this level of detail will be crucial to inform new strategies (and binding sites) for rational drug design for these drug targets.

KEYWORDS *EPR, Molecular Dynamics, Monoamine Oxidase B, semiquinone, enzyme, flavin, membrane*

Human monoamine Oxidase B (MAO-B) catalyzes the oxidative deamination of amines, by electron transfer, via its flavin adenine dinucleotide (FAD) cofactor (Scheme 1).[1] It is located in the outer mitochondrial membrane,[2] as a dimer, with bipartite substrate binding and active site cavities.[1] MAO-B is the target of treatment for both depression and Parkinson's disease, with inhibitors of the enzyme first being approved as pharmaceuticals in the 1960's.[3,4]

Despite the important medical applications associated with MAO-B its chemical mechanism remains unclear in the literature and there is debate over the role of MAO-B conformational change and protein dynamics. Reduction of the FAD has been shown to proceed by a tunneling mechanism via primary (1°) and secondary (2°) kinetic isotope effect (KIE) studies.[5] These studies have suggested that MAO-B catalysis is not linked to fast (pico/nanosecond) dynamics.[5,6] MAO-B catalysis has been investigated via experimental and computational studies, with at least seven different proposed mechanisms, including polar nucleophilic,[7] radical,[8] direct hydride transfer[9–11] and two step hydride transfer[12] (Scheme S1).

Although the direct single electron transfer (SET) radical mechanism (Scheme S1) has previously been discounted experimentally[13] and by quantum mechanics/molecular mechanics (QM/MM),[14] a separate radical mechanism has been proposed by Murray *et al*.[15] This was established via a model small molecule reaction that mimics MAO-B to provide evidence for a neutral semiquinone flavin that can be formed aerobically. The authors suggest that a neutral semiquinone flavin is the reactive species for the oxidation of benzylamine (BZA).[15] This led to the hypothesis of a radical mechanism whereby MAO-B forms a neutral semiquinone flavin via a proximal tyrosine radical (Y398). The presence of a stable anionic semiquinone flavin and tyrosyl radical intermediate are also reported in MAO-A and MAO-N.[16,17]

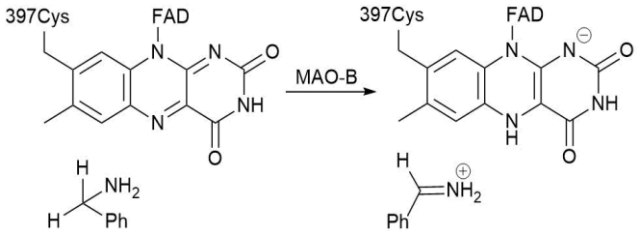

Scheme 1. General reaction catalyzed by MAO-B.

In our hands, we find spectroscopic evidence for a stable semiquinone in resting state MAO-B (*vida infra*). Here, MAO-B was expressed and purified in *Pichia pastoris* as outlined by Newton-Vinson *et al*. [18] This protocol attributes observations of oxidized/semiquinone MAO-B FAD to reactive oxygen species (ROS) that form upon the disruption of the mitochondrial membrane, which they observe upon purification from bovine liver, but *not* from *Pichia pastoris.*[18]

Previous observation of a stable anionic semiquinone FAD in MAO-B[19,20] led to a hypothesis of half-site reactivity. This mechanism posits that one monomer of the MAO-B dimer is inaccessible to oxygen and substrate, resulting in the formation of the stable semiquinone species, whilst the other contains oxidized FAD. Electrons are then shuttled to the semiquinone species, allowing for the oxidation of the reduced FAD upon turnover.[20] The authors suggest this might arise from electron shuttling between specific amino acids. Potentially such a mechanism might require significant conformational change associated with turnover in each monomer. Indeed, conformational changes have been found to be associated with MAO-B turnover, with a molecular dynamics (MD) study demonstrating the potential for the membrane to regulate access to the active site entrance via two gating loops (residues 85-119 and 155-165).[21] Other MD studies have been carried out on MAO-B, both with and without a membrane environment, with the focus on identifying or improving inhibitors for MAO-B[22–26], or ascertaining how MAO-B binds to the membrane.[27]

Herein, we find evidence for the validity of a resting anionic semiquinone, and through kinetic and computational studies, evidence for conformationally controlled enzyme activity at each MAO-B monomer. Crucially, we find that the membrane environment is the arbiter of this control mechanism and exposes novel substrate/product channels that could be potential new drug targets. We thereby link the membrane environment, substrate binding and MAO-B conformational change to enzyme turnover.

Results and Discussion

Evidence for a resting-state semiquinone in MAO-B. The absorption spectrum of purified MAO-B is shown in Figure 1. The spectra are characteristic of an anionic semiquinone FAD (FAD·-) with an absorption feature at ~415 nm.[28] The preparation protocol of MAO-B was the same as that used by Newton-Vinson *et al*.,[18] with small differences outlined in the materials and methods. Multiple preparations were completed, including the final polymer partition step outlined by Newton-Vinson *et al* and without EDTA present, with the ~415 nm spectral feature consistently present in our hands. The effect of incubation with BZA, under anaerobic conditions, on the MAO-B absorption feature at ~415 nm was monitored over time (Figure 1 *inset*). From Figure 1 *inset*, we find a decrease in absorption at 415nm with respect to time on incubation with BZA, suggesting the ~415 nm spectral feature is redox sensitive with a natural MAO-B substrate.

Potentially the ~415 nm absorption feature could be attributed to a tyrosyl radical, which has a characteristic absorbance peak at 410 nm,[29] or a mixture of both an FAD semiquinone and

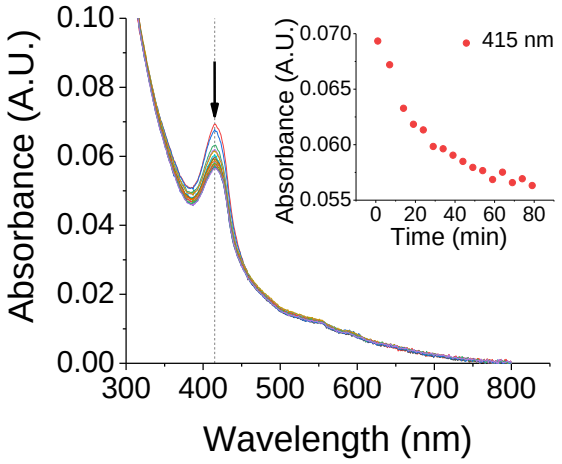

Figure 1. The absorbance spectra of MAO-B after treatment with BZA over time. *Inset*, the effect on the 415 nm peak over time. *Conditions*, 40 mM BZA, 50 mM HEPES 0.5 % w/v Triton X-100, 20 °C, anaerobic.

tyrosyl radical, as seen as intermediates in MAO-A.[16,17] Murray *et al.* postulated that the reactive semiquinone FAD was formed by a proximal tyrosyl radical (Y398). However, the UV-vis absorption spectrum of Y398F MAO-B shows the spectral feature at ~415 nm (Figure S1A), indicating that the observed spectral feature is not attributable to a Y398 tyrosyl radical. The Y398F variant also shows a slight increase in K_m (Figure S2), similar in magnitude to previously reported changes in K_m for Y398F.[30]

To resolve this spectral feature, EPR was used on both wildtype (WT) and Y398F MAO-B. The X-band spectrum of the WT MAO-B immediately indicates that the signal arises from a

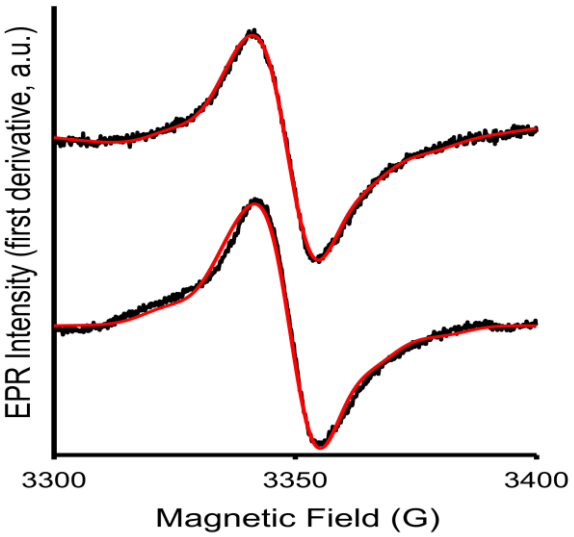

Figure 2. X-band cw-EPR spectra of WT (top, black) and Y398F (bottom, black) MAO-B, with their respective fitted simulations (red). EPR microwave frequency = 9.3916 GHz (WT) & 9.3926 GHz (Y398F), microwave power = 0.2 mW, modulation amplitude = 0.5 mT, temperature = 16 K.

Table 1. Spectral parameters of EPR data extracted by simulation and fitting.

		WT MAO-B	Y398F MAO-B
g-tensor	g_x	2.00444	2.00444
	g_y	2.00429	2.00429
	g_z	2.00191	2.00191
	g_{iso}	2.00355	2.00355
A(^{14}N) (MHz)	$A_{\parallel}$	39.3	38.4
	$A_{\perp}$	0	0
A(^{14}N) (MHz)	$A_{\parallel}$	34.1	40.1
	$A_{\perp}$	0	0
Linewidth (mT)		1.1	1.1
RMSD		0.0255	0.0440

semiquinone radical (Figure 2), in agreement with the UV-vis spectroscopy. The measured spectra lack the defining features which would identify the signal as arising from a tyrosyl radical: the typical 'wings' or 'shoulders' around the central signal at around g = 2 [16,31] at X-band (Figure 2), and increased g-value anisotropy at higher frequency (and therefore resonant field), i.e. Q-band (data not shown). Furthermore, the signal persists in the Y398F variant, confirming that it is not caused by the proximal tyrosine.

Computational simulation and fitting of the experimental X-band data of the WT and Y398F MAO-B (Table 1) suggests that the semiquinone radical species is anionic; the hyperfine environment of a neutral semiquinone radical would contain a contribution from an additional hydrogen atom.[20,32] This is not the case for the signals seen in the X-band spectra.

Previous studies have illustrated the importance of the membrane environment in mediating the normal enzymatic activity of MAO-B.[21] To probe if the putative semiquinoid species (inferred from spectroscopic studies above) was also stably present in the membrane environment, we have conducted spectroscopic studies in an artificial membrane environment using l-α-phosphatidylcholine styrene maleic acid co-polymer (SMA) nanodiscs, prepared as reported previously.[33] We find that the absorption feature at ~415 nm is present in both reduced triton X-100 and nanodisc environments (Figure S1A), implying that the putative anionic semiquinone is not an artifact of the buffer system used, and that its presence is not affected by the specific membrane environment used.

Influence of the membrane environment on MAO-B turnover. To assess how/if the membrane environment affects enzyme turnover, we measured MAO-B turnover with both BZA and kynuramine dihydrobromide (KYN) at a range of temperatures. We monitor enzyme turnover based on the absorption features of benzaldehyde product formation at 250 nm for BZA,[34] and 4-hydroxyquinoline product formation at 316 nm for KYN.[35] This assay notionally primarily reflects the rate of reduction of the flavin.[34] Our temperature dependence studies allow us to analyze not just the observed rate of enzyme turnover but also the thermodynamics of the system. The temperature-dependence of the observed rate is shown in Figure 3.

There has been a recent move to fitting enzyme temperature dependence data to physical models that allow for curvature in the associated plots. Such models often provide a more realistic fit to experimental data. We fit the MAO-B temperature dependence data to a model that incorporates the heat capacity of catalysis ($\Delta C_P^{\ddagger}$) (Eq 2) into the Eyring equation (Eq 1).[36]

$$k = \left(\frac{k_B T}{h}\right) e^{\frac{\Delta S^{\ddagger}}{R}} e^{-\frac{\Delta H^{\ddagger}}{RT}} \qquad \text{Eq 1}$$

$$lnk = ln\frac{k_B T}{h} - \left[\frac{\Delta H^{\ddagger}_{T_0} + \Delta C_P^{\ddagger}(T - T_0)}{RT}\right] + \left[\frac{\Delta S^{\ddagger}_{T_0} + \Delta C_P^{\ddagger}(lnT - lnT_0)}{R}\right] \qquad \text{Eq 2}$$

Where $\Delta H^{\ddagger}$ is the change in enthalpy and $\Delta S^{\ddagger}$ is the change in entropy between the ground and transition state of the reaction at an arbitrary reference temperature (T_0). This model has recently gained traction in studying enzyme temperature dependencies.[37–40] $\Delta C_P^{\ddagger}$ quantifies the temperature dependence

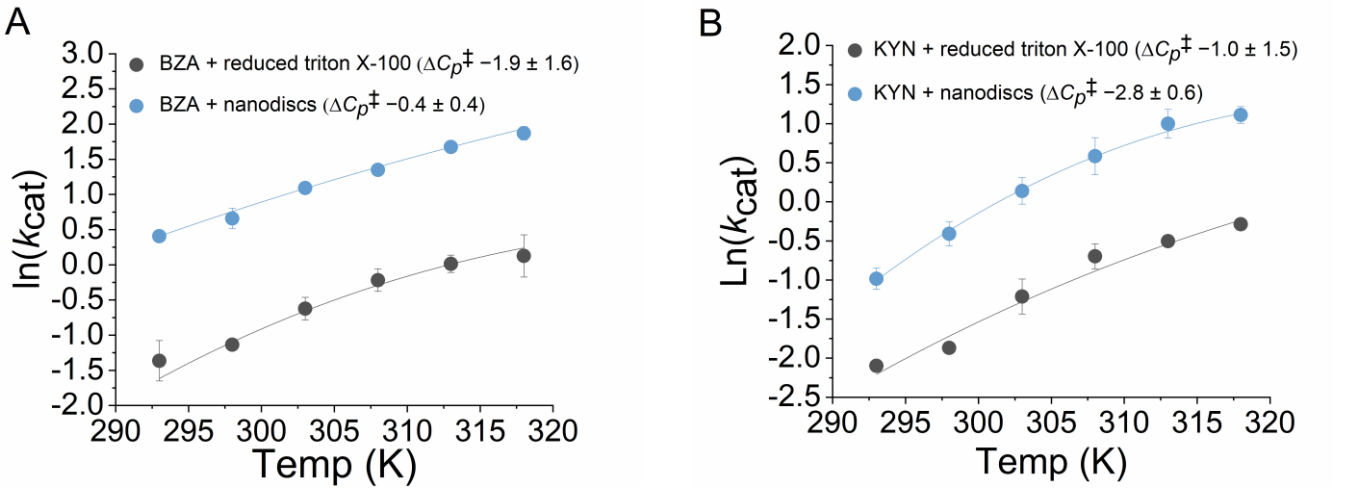

Figure 3. The temperature dependence of MAO-B with BZA (**A**) and KYN (**B**) with reduced triton and nanodisc environments, fit to the MMRT equation. *Conditions*, 50 mM HEPES 0.5 % w/v reduced triton X-100. Reduced triton X-100: 1.5 mM BZA, 0.75 mM KYN. Nanodiscs: 3 mM BZA, 0.66 mM KYN.

of $\Delta H^{\ddagger}$ and $\Delta S^{\ddagger}$ and reflects the difference in the distribution and frequency of vibrational modes between the ground state and transition state.[36,41] We have recently suggested that $\Delta C_P^{\ddagger}$ can be used as a proxy for the changes in these vibrational modes during enzyme turnover and thus relates to some aspect of the protein's molecular dynamics.[38] This is relevant in the present study where the membrane environment may not alter the tertiary structure of the enzyme, but potentially alters protein fluctuations, which have previously been proposed to affect small molecule binding to the active site.[21]

From Figure 3 and Table S1, we find $\Delta C_P^{\ddagger}$ to be the same within error for both KYN and BZA substrates when in a reduced triton X-100 environment. However, when in nanodiscs, the difference in $\Delta C_P^{\ddagger}$ for the different substrates is $\Delta\Delta C_P^{\ddagger} = 2.4 \pm 1.0$ kJ mol^{-1}. The $\Delta C_P^{\ddagger}$ increases in magnitude from reduced triton to nanodiscs with KYN, and decreases with BZA (Figure 3). These data suggest that the difference in conformational fluctuations in the reactant and transition states changes are different in a more native membrane environment and for different substrates. Moreover, we find a significant difference in the observed rate of enzyme turnover in the nanodiscs (~5 times faster). These data therefore provide experimental evidence of the notion that the membrane environment has a role in 'tuning' the molecular dynamics of MAO-B. However, given we observe a retention of the putative anionic flavin semiquinone, we would suggest the membrane does not affect the chemical mechanism of enzyme turnover *per se*.

To investigate if perturbing the dynamics or flexibility of MAO-B can lead to changes in turnover (as suggested by the difference in kinetics in reduced triton x-100 vs. nanodisc environment, see Figure 3), we have turned to computationally informed mutagenesis studies. We performed constraint analysis to identify both structural rigidity and the flexibility that permits large conformational changes,[42] which may occur on the nanosecond to millisecond timescale.[43] These calculations are based on an algorithm that defines a constraint-network of movement for a protein, by analyzing and interpreting the limits of hydrogen bonds, hydrophobic relations and the angles and lengths of single and double covalent bonds. From this, the degrees of movement can be balanced against the constraints, leading to the overall rigidity of the protein being established.[42]

By sequentially disregarding the side-chain contribution of MAO-B to its overall rigidity in the flexible motion calculations (see SI materials and methods), we identified residues that are likely to affect the flexibility of the enzyme. From these residues, we then selected three enzyme variants (W184F, E466Y and F402V) that, based on our calculations, were predicted to perturb the network of flexible motion, but are distal to the active site and catalytically relevant residues (Figure S3). We find that these variants retain the absorption feature at ~415 nm (Figure S1A) and their overall structure is not significantly perturbed, at least as assessed from their far-UV circular dichroism spectra (Figure S1B). However, despite the variants being located a significant distance from the active site, we find that enzyme activity is ablated. Given that these variants are expected to alter the network of flexible motion, we suggest these data reflect the importance of protein conformational changes in MAO-B turnover. Such changes point to a potential rationale for the differences of our temperature dependence studies when MAO-B is in different environments.

Computational evidence for a new entrance to the MAO-B active site mediated by the protein-membrane interaction. To obtain detailed insight into the role of the membrane environment on protein dynamics, we performed MD simulations of the MAO-B dimer embedded in a phospholipid membrane. We explore (i) the influence of the phospholipid membrane in modulating substrate/inhibitor binding, (ii) the accessibility of small molecules to the active site of MAO-B, and (iii) the potential for half-site reactivity, as discussed above.

MD simulations of MAO-B in complex with FAD in a POPC/POPE lipid bilayer (similar to the native environment in the mitochondrial membrane)[44] were performed in triplicate for 150 ns in 3 different states: no BZA present (BZA_0), one active site occupied with BZA (BZA_1), and both active sites occupied with BZA (BZA_2). Protein Cα RMSD and area per lipid head groups (Figure S4) indicated equilibration of both the protein and membrane after 50 ns of production MD. The analysis described below is therefore from 50 to 150 ns.

Prior simulations of BZA_0-MAO-B in a bilayer established that MAO-B ligand binding site access is modulated by the membrane.[21] We investigate this further using longer simulations (150 ns vs. 50 ns) and with substrate (BZA) bound. To measure possible access to the substrate cavity of MAO-B via the membrane, we quantify the occurrence and features of tunnels in our simulations using Caver 3.0.[45] Tunnels identified are grouped into clusters, allowing for the quantification of various characteristics, such as the frequency of occurrence and smallest width (bottleneck radius), as used here.[46] This tool has previously been used to identify tunnels for ligand-induced protein flexibility analysis,[47] to rationalize change in mechanism and kinetics of an enzyme upon a point mutation,[48] and to identify a tunnel to the FAD moiety in MAO-A.[49]

Two main possible entrances for ligands into the MAO-B active site are found at either side of the gating loop residues 99 to 112 (Figure 4). Entrance A (Figure 4A) is accessed via the membrane and its opening has previously been observed.[21] Briefly, a π-π stacking interaction between Tyr97 and Trp107 is lost as Trp107 buries into the aliphatic lipid tails of the bilayer, establishing an additional interaction of MAO-B with the phospholipid bilayer.

Entrance B (Figure 4B) is solvent accessible, and its opening is controlled by the conformation of three loop regions (81 to 88, 99 to 112 and 198 to 208). To the best of our knowledge, its opening has not yet been observed through protein crystallography or simulation. To provide a qualitative description of the open and closed conformations of this entrance, we have performed clustering analysis on the entrance loop residues (see Materials and Methods). Opening of Entrance B (Figure S5 A,B) can be described by: 1) loop 81-88 separates from loop 199-206, breaking a number of transiently formed electrostatic interactions and instead forming interactions with the solvent in the open conformation; 2) the

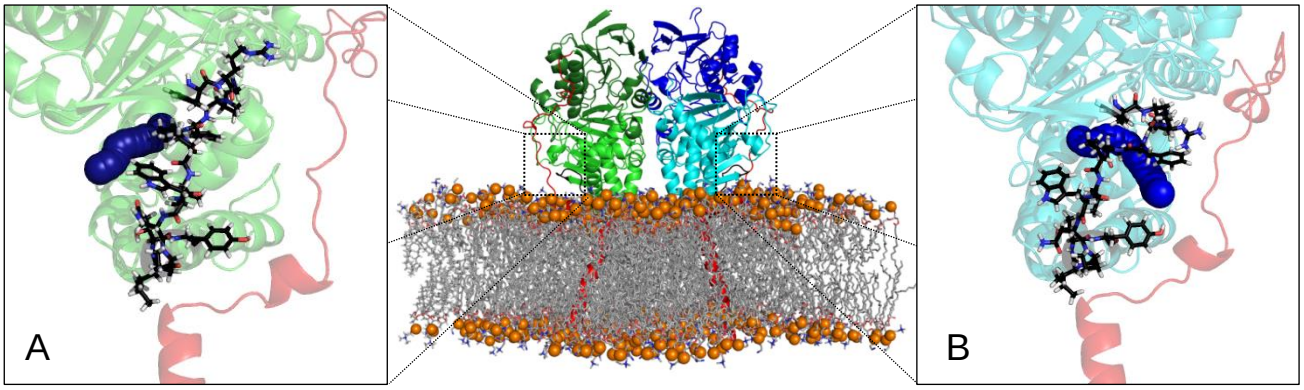

Figure 4. MAO-B in POPC/POPE membrane environment. The substrate binding area is shown in light green and light blue (residues 80-210, 286-390, and 454-488). The active site area is shown in dark green and dark blue (residues 4-79, 211-285, and 391-435). The membrane binding region is shown in red (residues 489-500). The binding site gating loop is shown in black (residues 99-122). The navy spheres on the left and the right are the two main entrances (or tunnels) to the binding site (as identified by Caver 3.0 [45]). Entrance B is newly identified here, Entrance A has been previously described.[21]

central region of the gating loop (residues P102, F103, P104) rotates down and away from the hydrophobic core of the entrance cavity. The opening of both entrance A and B involves residues directly interacting with the bilayer. This indicates that the membrane is important in modulating access to the substrate binding pocket of MAO-B.

Evidence of asymmetry in MAO-B from MD simulation. Previous studies have suggested that the presence of an anionic semiquinone could be mechanistically significant as part of a half-site reactivity mechanism.[20] To investigate the potential for half-site reactivity in MAO-B, tunnels from the N5 of the flavin to the solvent were first identified from all MD trajectories with BZA_0, BZA_1 and BZA_2 (with three replicates). These data are useful to determine the size of species that could access the active site and to investigate whether access to the active site is half-site specific. To avoid identifying numerous tunnels that cannot accommodate substrate/product molecules, a minimum tunnel radius was set to 1.5 Å. (This avoids identifying water tunnels, as water has a Van der Waals radius of ~1.4 Å.[50]) With this criterion, no tunnels were found, which demonstrates a closed active-site on the timescales of our simulations. Whilst larger conformational changes may be occurring on longer time-scales (or in presence of substrate in the vicinity of a bottleneck) to enable substrate access to the active site, a generally closed off active site is in agreement with previous experimental findings.[20]

Next, tunnels were identified from the substrate binding cavity towards the protein surface. The starting point was defined as the center of mass between the alpha carbon (Cα) atoms of residues 168 and 316 (Figure S6). This starting point was chosen as it is located within the substrate binding cavity and is common to both previously described substrate entrance tunnels (Figure 4). Tunnel frequency and the average bottleneck radius of all tunnels identified in both monomers were obtained for BZA_0 and BZA_1 (Figure 5 A,B). To aid discussion, we designate each monomer as monomer 1 or monomer 2, noting that this does not imply a structural or other difference between monomers.

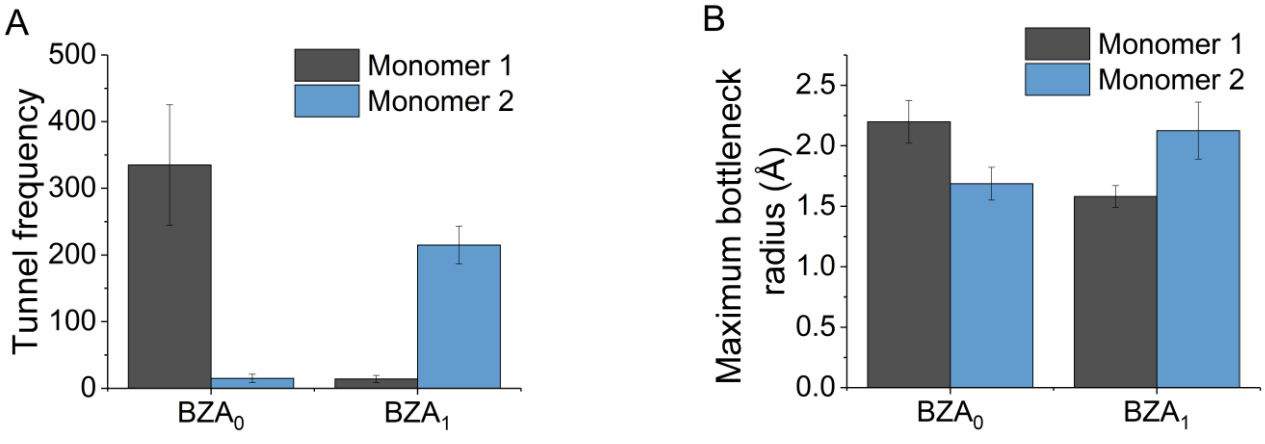

Figure 5. A. The summed tunnel frequency from the substrate binding site of MAO-B to solvent, identified by caver. BZA_0 – No BZA is bound in either monomer. BZA_1 – BZA is bound only in monomer 1. All are from triplicate MD runs. **B.** The average maximum bottleneck (Å) from substrate binding site of MAO-B to solvent, identified by caver. Same conditions as panel A.

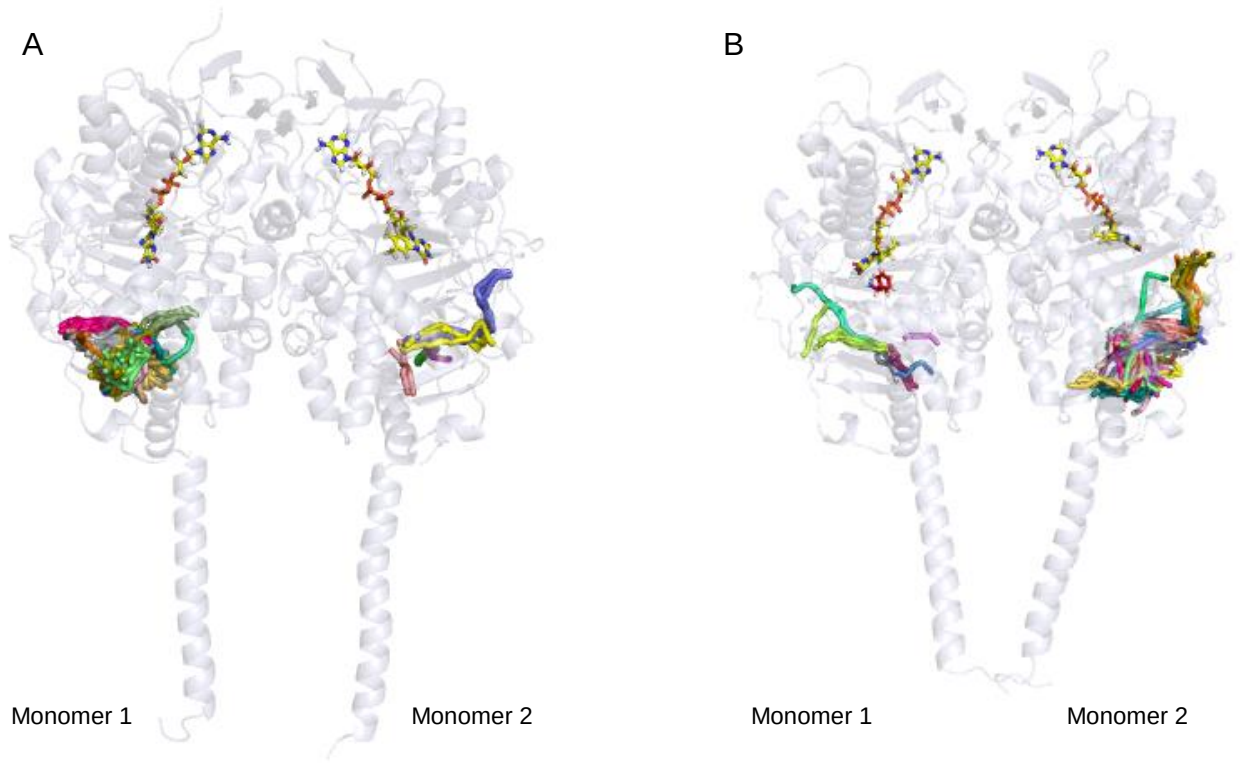

Figure 6. All tunnels identified by caver over all three MD simulation repeats, for the binding site of MAO-B, with FAD cofactor shown as yellow sticks. A. Without substrate bound (BZA_0). B. With BZA in monomer 1 (shown as red sticks), and not monomer 2 (BZA_1).

Notably, both the frequency and maximum bottleneck radius of tunnels to the substrate binding cavity of MAO-B is significantly different for each monomer. In the absence of BZA, monomer 1 presents a higher frequency of tunnels, with a larger average maximum bottleneck radius. When BZA is present in its catalytically competent conformation in monomer 1 and not monomer 2, the frequency of tunnels and maximum bottleneck measurements are higher for monomer 2 (Figure 5A,B, Figure 6 and Table S2). At Figure 6 the different colours show different routes from the starting point to the solvent, with the majority of tunnels passing the aforementioned entrances A and B (Figure 4). Asymmetry between the monomers was also observed in the flexibility of the binding site gating loop (residues 95-115): it was found to be significantly more flexible in the $BZA_{1\text{-unbound}}$ monomer than in the $BZA_{1\text{-bound}}$ and BZA_0 monomers (Figure S7).

The observed 'closing' of the active site entrance in the $BZA_{1\text{-bound}}$ monomer and 'opening' in the $BZA_{1\text{-unbound}}$ monomer are particularly notable. This indicates that when BZA is bound to the active site cavity of one monomer, a subsequent BZA is more likely to enter the binding site of the opposite monomer. Such asymmetry may prevent binding of subsequent BZA into the same monomer, allowing for the release of products, whilst increasing the efficiency of binding in the opposite 'free' monomer. Previous experimental work indicated that binding of inhibitor to the intermediate binding site of MAO-B was increased where inhibitor was already bound into the active site (see Figure 4 for binding/active site differentiation).[51] Whilst it is not known whether this is within the same monomer, it could explain the asymmetry in binding site access seen here when BZA_1 is present.

BZA_2 was not considered for half-site reactivity analysis. This was due to BZA leaving the active site altogether in one simulation trajectory (Figure S8), meaning that the identified tunnels would not be comparable to those where BZA does not leave. This BZA movement may indicate, however, that BZA_2 is potentially an unstable configuration, providing further evidence towards asymmetry in MAO-B.

Conclusions

MAO-B is an important biomedical target, and as with many such targets, is associated with a biological membrane. Such association places enzymes in specific physiological contexts, can promote interaction with other species and enable specific structural features. Less obvious is the role of the membrane environment in mediating the conformational dynamics of enzymes, and whether this is functionally important.

Previous molecular dynamics studies have illustrated that the immediate membrane environment of MAO-B is involved in controlling substrate entrance to channels leading to the active site. Here, using enzyme kinetic and mutagenesis studies, we consider the role of the membrane environment in tuning the molecular dynamics of MAO-B more widely, including its influence on turnover and catalysis. We find that placement of MAO-B in SMA nanodiscs instead of in reduced triton X-100 has a significant effect on the heat capacity of catalysis ($\Delta C_P^{\ddagger}$). Differences in $\Delta C_P^{\ddagger}$ reflect differences in the distribution and

frequency of vibrational modes between the ground (reactant) and transition states and implies that the membrane environment is affecting the global protein dynamics of MAO-B *and* that these dynamics influence the thermodynamics of enzyme turnover. Indeed, k_{cat} is ~5 times faster in the nanodisc environment versus reduced triton X-100. These data further hint at the role of the specific lipid composition and fine structure of the membrane to tune MAO-B turnover efficiency. These findings are corroborated by studying enzyme variants that are predicted to alter the network of flexible motion in the enzyme, but do not affect the overall structure. These variants, which are distal to the active site, all lead to inactive enzyme, indicating the critical role of 'optimized' global protein dynamics of MAO-B.

Through atomistic molecular dynamics simulations with and without substrate bound, we find two substrate entrance/product exit channels that are mediated by membrane interaction, one of which was not previously described. The simulations further indicate an asymmetry in substrate access in the MOA-B dimer. Specifically, either one or the other monomer may allow substrate access at any one time, with active site occupation in one monomer preferentially allowing substrate access to the other.

Taken together, our study suggests that the global protein dynamics of MAO-B are 'tuned' by the specific immediate membrane environment. These protein dynamics have a major effect on MAO-B function, through tuning fluctuations linked to enzyme turnover, but also in controlling the opening and closing of substrate/product channels. The finding that two different channels mediated by the membrane environment are present in MAO-B illustrates the potential to exploit novel small molecule binding sites with rational drug design. That is, our study illustrates that when searching for novel small molecule binding sites one should consider not just static structure and the experimental system in isolation, but time-dependent changes in the population of conformational sub-states and in the 'native' environment.

Experimental materials and methods

Unless otherwise stated, all reagents were obtained from Sigma-Aldrich.

MAO-B expression and purification. MAO-B was expressed and purified following the purification protocol by Newton-Vinson *et al*.[18] Small variations from the protocol include shake flask fermentation instead of bioreactor fermentation, with BMMY (buffered methanol-complex medium) media instead of MM (minimal methanol) media for induction, storage of cell pellets in a buffer with protease inhibitor tablets instead of PMSF, suspension of pellet in 100 ml of breaking buffer instead of 1 L, and cell breakage of 30 s on 30 s off x 10 sonication in addition to bead beating. The purification was completed after MAO-B was passed over a DEAE-sepharose FF column, achieving satisfactory purity. The additional polymer partition step detailed by Newton-Vinson et al.[18] did not change the state of the semiquinone MAO-B species seen here, with additional purity achieved by size exclusion chromatography if necessary.

Nanodisc preparation. Nanodiscs were prepared following methods by McDowall *et al*.,[33] suspended in 50 mM HEPES, pH 7.5. and incubated with MAO-B in a 10x molar excess, for 2 hours prior to experiments.

Enzyme assays. MAO-B was transferred from Triton X-100 containing buffer to reduced triton X-100 or nanodisc containing buffer using detergent removal spin columns (Thermo Scientific Pierce). Steady-state MAO-B kinetic measurements were carried out using a 1 ml quartz cuvette and a UV⁄ Vis spectro-photometer (Agilent Cary 60 UV-Vis spectrometer) in 50 mM HEPES (pH 7.5), containing 0.5 % (w/v) reduced Triton X-100 or SMA l-α-Phosphatidylcholine nanodiscs. Enzyme activity was measured by following the formation of benzaldehyde using ε_{250} = 12,800 M^{-1} cm^{-1} for BZA,[34] and 4-hydroxyquinoline using ε_{316} = 12,300 M^{-1} cm^{-1} for KYN.[35] For each condition substrate dependences were monitored at 40 °C ; the data fitted well to Michaelis-Menten kinetics (Figure S9). Temperature dependences were carried out from 20 °C - 45 °C at 5 °C intervals using initial velocity measurements at substrate concentrations maintained above 10x K_m to ensure saturation. The data were fitted to Eq 2 as described in the manuscript using OriginPro 2017.

Redox assays. These experiments were performed anaerobically, all buffer was purged with nitrogen and samples were prepared in an anaerobic box. Glucose and glucose oxidase were added to maintain anaerobic conditions.

EPR. Measurements were performed using WT and Y398F variant MAO-B in 50 mM HEPES 0.5% Triton, pH 7.5, flash-frozen in liquid nitrogen in suprasil quartz sample tubes. X-band cw-EPR spectra were recorded on a Bruker eleXsys E500 spectrometer using a standard rectangular Bruker EPR cavity (ER4102T) equipped with an Oxford helium cryostat (ESR900). Experimental parameters: microwave power, 0.2 mW; field modulation amplitude, 5 G; field modulation frequency, 100 kHz; measuring time 10 s; temperature 16 K. Q-band cw-EPR spectra were performed on a Bruker eleXsys E-560 spectrometer using a ER 5106QT-W1 resonator equipped with a home-built ARS cryogen-free cryostat (data not shown). Spectral simulations were performed using the Matlab-based Easyspin package.[52]

Computational materials and methods. The X-ray crystal structure of MAO-B in complex with 6-hydroxy-N-propargyl-1(R)-aminoindan (1S3E)[53] was used as the starting point for all MD simulations. The missing C-terminal residues (502 – 520 Chain A and 497 – 520 Chain B) which form the remainder of the transmembrane helix were built using Avogadro[54] (assuming the standard backbone dihedral angles of an α-helix). MAO-B was then inserted into a lipid bilayer comprised of a 4:3 ratio of palmitoyloleoylphosphatidylcholine (POPC) and palmitoyloleoyl-phosphatidylethanolamine (POPE) using CHARMM-GUI.[55] This composition has been used in prior bilayer MD simulations of MAO-B, and was chosen to represent the composition of the outer mitochondrial membrane.[21,27,44] BZA was placed in the active site by alignment with the crystal structure of MAO-B in complex with nitrobenzylamine (2C70,[56] Cα RMSD 0.118 Å to 1S3E; the latter was used due to its higher resolution). All simulations of

BZA were performed with the amino group in its neutral form, as this is widely believed to be the catalytically competent state of BZA.[13,14,57] Titratable residues were simulated in their standard protonation states, based on calculations with PropKa 3.0[58]. MolProbity was used to determine the optimum tautomerisation states of every His residue, and any required Asn/Gln side chain flips, based on optimizing the hydrogen bonding network[59]. Histidines 91, 115 and 452 were singly protonated on their Nδ1, with all others singly protonated on their Nε2. The system was then solvated such that there was no protein or lipid atom within 20 Å of the edge of the periodic box along the z-coordinate (bilayer normal). The total number of atoms for each system simulated was approximately 90,000.

Periodic boundary simulations were performed with Amber16, using the CHARMM36 force field to describe protein[60] and lipid[61] atoms, and TIP3P for water. Parameters for FAD in its oxidized form and BZA in its neutral form were taken from Abad *et al.*[14] Following minimization, heating and equilibration (see SI Materials and Methods), production MD simulations were run in the NpT ensemble at 310 K, with semi-isotropic coupling to a Monte Carlo barostat. Temperature was regulated using Langevin dynamics with a collision frequency of 1 ps^{-1}. A time step of 2 fs was applied with the covalent bonds to hydrogen constrained by the SHAKE algorithm. A 12 Å non-bonded cut-off was applied with a force switch smoothing function from 10 to 12 Å. Long range electrostatics were evaluated with the particle mesh Ewald method.[62] A total of 9 simulations were performed for 150 ns each, with the first 50 ns of simulation used as equilibration. The BZA_2 run in which a BZA escapes the active site cavity was extended for a further 50 ns. Coordinates were saved every 10 ps for further analysis.

Routine analysis of trajectories was performed using cpptraj from the AmberTools suite.[63] Area per lipid calculations were performed with GridMAT-MD,[64] using a grid resolution of 200 x 200 points for each measurement. Tunnel analysis was performed with Caver 3.0[45]. All settings were kept default apart from bottleneck radius (1.5 Å).

ASSOCIATED CONTENT

Supporting Information. FIRST calculations methodology, molecular dynamics simulation methodology, MAO-B mechanisms, table of caver data, MAO-B mutant and environment spectra, Michealis-Menten of Y398F MAO-B, MD RMSD and area per lipid calculations, Entrance B structure, Caver calculation starting point, RMSF of gating loop, BZA leading the active site by MD simulations, Michaelis-Mentens of WT MAO-B.

AUTHOR INFORMATION

Corresponding Authors

*Christopher R Pudney, Department of Biology and Biochemistry, University of Bath, Bath, United Kingdom. c.r.pudney@bath.ac.uk.
*Marc W van der Kamp, School of Biochemistry, University of Bristol, Cantock's Close, Bristol BS8 1TS, United Kingdom. marc.vanderkamp@bristol.ac.uk.

Author Contributions

HBLJ and AM performed experimental work. HBLJ and RMC performed computational calculations and simulations. All authors discussed and interpreted data. The manuscript was written through contributions of all authors. All authors have given approval to the final version of the manuscript.

ABBREVIATIONS

Alpha carbon (Cα), benzylamine (BZA), electron paramagnetic resonance (EPR), flavin adenine dinucleotide (FAD), heat capacity of catalysis ($\Delta C_P^{\ddagger}$), kynuramine (KYN), molecular dynamics (MD), monoamine oxidase (MAO), palmitoyloleoylphosphatidylcholine (POPC), palmitoyloleoyl-phosphatidylethanolamine (POPE), root mean square fluctuation (RMSF), reactive oxygen species (ROS).

ACKNOWLEDGMENT

HBLJ's studentship is funded by the University of Bath. RMC's studentship is funded by the EPSRC. MWvdK is a BBSRC David Phillips Fellow (BB/M026280/1). SAW has received funding from the European Research Council (ERC) under the European Union's Horizon 2020 research and innovation programme (grant agreement No 648283 "GROWMOF")

REFERENCES

(1) Binda, C.; Newton-Vinson, P.; Hubálek, F.; Edmondson, D. E.; Mattevi, A. Structure of Human Monoamine Oxidase B, a Drug Target for the Treatment of Neurological Disorders. *Nat. Struct. Biol.* **2002**, *9*, 22–26.

(2) Schnaitman, C.; Erwin, V. G.; Greenawalt, J. W. The Submitochondrial Localization of Monoamine Oxidase. An Enzymatic Marker for the Outer Membrane of Rat Liver Mitochondria. *J. Cell Biol.* **1967**, *32*, 719–735.

(3) Knoll, J.; Ecseri, Z.; Kelemen, K.; Nievel, J.; Knoll, B. Phenylisopropylmethylpropinylamine (E-250), a New Spectrum Psychic Energizer. *Arch. Int. Pharmacodyn. Ther.* **1965**, *155*, 154–164.

(4) Riederer, P.; Laux, G. MAO-Inhibitors in Parkinson's Disease. *Exp. Neurobiol.* **2011**, *20*, 1–17.

(5) Jonsson, T.; Edmondson, D. E.; Klinman, J. P. Hydrogen Tunneling in the Flavoenzyme Monoamine Oxidase B. *Biochemistry* **1994**, *33*, 14871–14878.

(6) Nagel, Z. D.; Klinman, J. P. Tunneling and Dynamics in Enzymatic Hydride Transfer. *Chem. Rev.* **2006**, *106*, 3095–3118.

(7) MacMillar, S.; Edmondson, D. E.; Matsson, O. Nitrogen Kinetic Isotope Effects for the Monoamine Oxidase B-Catalyzed Oxidation of Benzylamine and (1,1-$^2H_2$)Benzylamine: Nitrogen Rehybridization and CH Bond Cleavage Are Not Concerted. *J. Am. Chem. Soc.* **2011**, *133*, 12319–12321.

(8) Lu, X.; Rodriguez, M.; Ji, H.; Silverman, R.; Vintem, A. P. B.; Ramsay, R. R. Chapman S, Perham R, Scrutton N, Editors. *Irreversible Inact. mitochondrial monoamine oxidases. Flavins Flavoproteins* **2002**, 817–830.

(9) Akyüz, M. A.; Erdem, S. S. Computational Modeling of the Direct Hydride Transfer Mechanism for the MAO Catalyzed Oxidation of Phenethylamine and Benzylamine: ONIOM (QM/QM) Calculations. *J. Neural Transm.* **2013**, *120*, 937–945.

(10) Kurtz, K. A.; Rishavy, M. A.; Cleland, W. W.; Fitzpatrick, P. F. Nitrogen Isotope Effects as Probes of the Mechanism of D-Amino Acid Oxidase. *J. Am. Chem. Soc.* **2000**, *122*, 12896–12897.

(11) Fitzpatrick, P. F. Oxidation of Amines by Flavoproteins. *Arch. Biochem. Biophys.* **2010**, *493*, 13–25.

(12) Vianello, R.; Repič, M.; Mavri, J. How Are Biogenic Amines Metabolized by Monoamine Oxidases? *European J. Org. Chem.* **2012**, *2012*, 7057–7065.

(13) Silverman, R. B. Radical Ideas about Monoamine Oxidase. *Acc. Chem. Res* **1995**, *28*, 335–342.

(14) Abad, E.; Zenn, R. K.; Kästner, J. Reaction Mechanism of Monoamine Oxidase from QM/MM Calculations. *J. Phys. Chem. B* **2013**, *117*, 14238–14246.

(15) Murray, A. T.; Dowley, M. J. H.; Pradaux-Caggiano, F.; Baldansuren, A.; Fielding, A. J.; Tuna, F.; Hendon, C. H.; Walsh, A.; Lloyd-Jones, G. C.; … Carbery, D. R. Catalytic Amine Oxidation under Ambient Aerobic Conditions: Mimicry of Monoamine Oxidase B. *Angew. Chemie Int. Ed.* **2015**, *54*, 8997–9000.

(16) Rigby, S. E. J.; Hynson, R. M. G.; Ramsay, R. R.; Munro, A. W.; Scrutton, N. S. A Stable Tyrosyl Radical in Monoamine Oxidase A. *J. Biol. Chem.* **2005**, *280*, 4627–4631.

(17) Dunn, R. V.; Munro, A. W.; Turner, N. J.; Rigby, S. E. J.; Scrutton, N. S. Tyrosyl Radical Formation and Propagation in Flavin Dependent Monoamine Oxidases. *ChemBioChem* **2010**, *11*, 1228–1231.

(18) Newton-Vinson, P.; Hubalek, F.; Edmondson, D. E. High-Level Expression of Human Liver Monoamine Oxidase B in Pichia Pastoris. *Protein Expr. Purif.* **2000**, *20*, 334–345.

(19) Yue, K. T.; Bhattacharyya, A. K.; Zhelyaskov, V. R.; Edmondson, D. E. Resonance Raman Spectroscopic Evidence for an Anionic Flavin Semiquinone in Bovine Liver Monoamine Oxidase. *Arch. Biochem. Biophys.* **1993**, *300*, 178–185.

(20) DeRose, V. J.; Woo, J. C. G.; Hawe, W. P.; Hoffman, B. M.; Silverman, R. B.; Yelekci, K. Observation of a Flavin Semiquinone in the Resting State of Monoamine Oxidase B by Electron Paramagnetic Resonance and Electron Nuclear Double Resonance Spectroscopy. *Biochemistry* **1996**, *35*, 11085–11091.

(21) Allen, W. J.; Bevan, D. R. Steered Molecular Dynamics Simulations Reveal Important Mechanisms in Reversible Monoamine Oxidase B Inhibition. *Biochemistry* **2011**, *50*, 6441–6454.

(22) Is, Y. S.; Durdagi, S.; Aksoydan, B.; Yurtsever, M. Proposing Novel MAO-B Hit Inhibitors Using Multidimensional Molecular Modeling Approaches and Application of Binary QSAR Models for Prediction of Their Therapeutic Activity, Pharmacokinetic and Toxicity Properties.

(23) Braun, G. H.; M Jorge, D. M.; Ramos, H. P.; Alves, R. M.; da Silva, V. B.; Giuliatti, S.; Vilela Sampaio, S.; Taft, C. A.; T P Silva, C. H. Molecular Dynamics, Flexible Docking, Virtual Screening, ADMET Predictions, and Molecular Interaction Field Studies to Design Novel Potential MAO-B Inhibitors. *J. Biomol. Struct. Dyn.* **2008**, *254*, 347–355.

(24) La Regina, G.; Silvestri, R.; Artico, M.; Lavecchia, A.; Novellino, E.; Befani, O.; Turini, P.; Agostinelli, E. New Pyrrole Inhibitors of Monoamine Oxidase: Synthesis, Biological Evaluation, and Structural Determinants of MAO-A and MAO-B Selectivity. *J. Med. Chem.* **2007**, *50*, 922–931.

(25) Maccioni, E.; Alcaro, S.; Cirilli, R.; Vigo, S.; Cardia, M. C.; Sanna, M. L.; Meleddu, R.; Yanez, M.; Costa, G.; … Distinto, S. 3-Acetyl-2,5-Diaryl-2,3-Dihydro-1,3,4-Oxadiazoles: A New Scaffold for the Selective Inhibition of Monoamine Oxidase B. *J. Med. Chem.* **2011**, *54*, 6394–6398.

(26) Chimenti, F.; Maccioni, E.; Secci, D.; Bolasco, A.; Chimenti, P.; Granese, A.; Befani, O.; Turini, P.; Alcaro, S.; … Distinto, S. Synthesis, Molecular Modeling Studies, and Selective Inhibitory Activity against Monoamine Oxidase of 1-Thiocarbamoyl-3,5-Diaryl-4,5-Dihydro-(1H)- Pyrazole Derivatives. *J. Med. Chem.* **2005**, *48*, 7113–7122.

(27) Fowler, P. W.; Balali-Mood, K.; Deol, S.; Coveney, P. V.; Sansom, M. S. P. Monotopic Enzymes and Lipid Bilayers: A Comparative Study. *Biochemistry* **2007**, *46*, 3108–3115.

(28) Kao, Y. T.; Saxena, C.; He, T. F.; Guo, L.; Wang, L.; Sancar, A.; Zhong, D. Ultrafast Dynamics of Flavins in Five Redox States. *J. Am. Chem. Soc.* **2008**, *130*, 13132–13139.

(29) Candeias, L. P.; Turconi, S.; Nugent, J. H. A. Tyrosine Y(Z) and Y(D) of Photosystem II Comparison of Optical Spectra to Those of Tyrosine Oxidised by Pulsed Radiolysis. *Biochim. Biophys. Acta - Bioenerg.* **1998**, *1363*, 1–5.

(30) Geha, R. M.; Chen, K.; Wouters, J.; Ooms, F.; Shih, J. C. Analysis of Conserved Active Site Residues in Monoamine Oxidase A and B and Their Three-Dimensional Molecular Modeling. *J. Biol. Chem.* **2002**, *277*, 17209–17216.

(31) Aubert, C.; Brettel, K.; Mathis, P.; Eker, A. P. M.; Boussac, A. EPR Detection of the Transient Tyrosyl Radical in DNA Photolyase from *Anacystis Nidulans*. *J. Am. Chem. Soc.* **1999**, *121*, 8659–8660.

(32) Okafuji, A.; Schnegg, A.; Schleicher, E.; Möbius, K.; Weber, S. G-Tensors of the Flavin Adenine Dinucleotide Radicals in Glucose Oxidase: A Comparative Multifrequency Electron Paramagnetic Resonance and Electron−Nuclear Double Resonance Study. *J. Phys. Chem. B* **2008**, *112*, 3568–3574.

(33) McDowall, J. S.; Ntai, I.; Hake, J.; Whitley, P. R.; Mason, J. M.; Pudney, C. R.; Brown, D. R. Steady-State Kinetics of α-Synuclein Ferrireductase Activity Identifies the Catalytically Competent Species. *Biochemistry* **2017**, *56*, 2497–2505.

(34) Walkers, M. C.; Edmondson ', D. E. Structure-Activity Relationships in the Oxidation of Benzylamine Analogues by Bovine Liver Mitochondrial Monoamine Oxidase B+,I. *7088 Biochem.* **1994**, *33*, 7088–7098.

(35) Weyler, W.; Salach, J. I. Purification and Properties of Mitochondrial Monoamine Oxidase Type A from Human Placenta. *J. Biol. Chem.* **1985**, *260*, 13199–13207.

(36) Hobbs, J. K.; Jiao, W.; Easter, A. D.; Parker, E. J.; Schipper, L. a.; Arcus, V. L. Change in Heat Capacity for Enzyme Catalysis Determines Temperature Dependence of Enzyme Catalyzed Rates. *ACS Chem. Biol.* **2013**, *8*, 2388–2393.

(37) Jones, H. B.; Wells, S. A.; Prentice, E. J.; Kwok, A.; Liang, L. L.; Arcus, V. L.; Pudney, C. R. A Complete Thermodynamic Analysis of Enzyme Turnover Links the Free Energy Landscape to Enzyme Catalysis. *FEBS J.* **2017**.

(38) van der Kamp, M. W.; Prentice, E. J.; Kraakman, K. L.; Connolly, M.; Mulholland, A. J.; Arcus, V. L. Dynamical Origins of Heat Capacity Changes in Enzyme-Catalysed Reactions. *Nat. Commun.* **2018**, *9*, 1177.

(39) Jones, H. B. L.; Crean, R. M.; Matthews, C.; Troya, A. B.; Danson, M. J.; Bull, S. D.; Arcus, V. L.; van der Kamp, M. W.;

Pudney, C. R. Uncovering the Relationship between the Change in Heat Capacity for Enzyme Catalysis and Vibrational Frequency through Isotope Effect Studies. *ACS Catal.* **2018**, *8*, 5340–5349.

(40) Longbotham, J. E.; Hardman, S. J. O.; Gö, S.; Scrutton, N. S.; Hay, S. Untangling Heavy Protein and Cofactor Isotope Effects on Enzyme-Catalyzed Hydride Transfer. *J. Am. Chem. Soc* **2016**, *138*, 13693–13699.

(41) Arcus, V. L.; Prentice, E. J.; Hobbs, J. K.; Mulholland, A. J.; van der Kamp, M. W.; Pudney, C. R.; Parker, E. J.; Schipper, L. A. On the Temperature Dependence of Enzyme-Catalyzed Rates. *Biochemistry* **2016**, *55*, 1681–1688.

(42) Wells, S.; Jimenez-Roldan J. E.; Römer, R. A. Comparative analysis of rigidity across protein families. *Phys. Biol.* **2009**, *6*. 046005.

(43) Ho, B. K.; Agard, D. A. Probing the Flexibility of Large Conformational Changes in Protein Structures through Local Perturbations. *PLoS Comput. Biol.* **2009**, *5*, e1000343.

(44) van Meer, G.; Voelker, D. R.; Feigenson, G. W. Membrane Lipids: Where They Are and How They Behave. *Nat. Rev. Mol. Cell Biol.* **2008**, *9*, 112–124.

(45) Chovancova, E.; Pavelka, A.; Benes, P.; Strnad, O.; Brezovsky, J.; Kozlikova, B.; Gora, A.; Sustr, V.; Klvana, M.; … Damborsky, J. CAVER 3.0: A Tool for the Analysis of Transport Pathways in Dynamic Protein Structures. *PLoS Comput. Biol.* **2012**, *8*, e1002708.

(46) Pavelka, A.; Sebestova, E.; Kozlikova, B.; Brezovsky, J.; Sochor, J.; Damborsky, J. CAVER: Algorithms for Analyzing Dynamics of Tunnels in Macromolecules. *IEEE/ACM Trans. Comput. Biol. Bioinforma.* **2016**, *13*, 505–517.

(47) Kingsley, L. J.; Lill, M. A. Including Ligand-Induced Protein Flexibility into Protein Tunnel Prediction. *J. Comput. Chem.* **2014**, *35*, 1748–1756.

(48) Biedermannová, L.; Prokop, Z.; Gora, A.; Chovancová, E.; Kovács, M.; Damborský, J.; Wade, R. C. A Single Mutation in a Tunnel to the Active Site Changes the Mechanism and Kinetics of Product Release in Haloalkane Dehalogenase LinB. *J. Biol. Chem.* **2012**, *287*, 29062–29074.

(49) Zapata-Torres, G.; Fierro, A.; Miranda-Rojas, S.; Guajardo, C.; Saez-Briones, P.; Salgado, J. C.; Celis-Barros, C. Influence of Protonation on Substrate and Inhibitor Interactions at the Active Site of Human Monoamine Oxidase-A. *J. Chem. Inf. Model.* **2012**, *52*, 1213–1221.

(50) Tabbutt, F. Water: A Matrix of Life, 2nd Edition (Franks, Felix). *J. Chem. Educ.* **2001**, *78*, 593.

(51) Bonivento, D.; Milczek, E. M.; McDonald, G. R.; Binda, C.; Holt, A.; Edmondson, D. E.; Mattevi, A. Potentiation of Ligand Binding through Cooperative Effects in Monoamine Oxidase B. *J. Biol. Chem.* **2010**, *285*, 36849–36856.

(52) Stoll, S.; Schweiger, A. EasySpin, a Comprehensive Software Package for Spectral Simulation and Analysis in EPR. *J. Magn. Reson.* **2006**, *178*, 42–55.

(53) Binda, C.; Hubálek, F.; Li, M.; Herzig, Y.; Sterling, J.; Edmondson, D. E.; Mattevi, A. Crystal Structures of Monoamine Oxidase B in Complex with Four Inhibitors of the N-Propargylaminoindan Class. *J. Med. Chem.* **2004**, *47*, 1767–1774.

(54) Hanwell, M. D.; Curtis, D. E.; Lonie, D. C.; Vandermeersch, T.; Zurek, E.; Hutchison, G. R. Avogadro: An Advanced Semantic Chemical Editor, Visualization, and Analysis Platform. *J. Cheminform.* **2012**, *4*, 17.

(55) Wu, E. L.; Cheng, X.; Jo, S.; Rui, H.; Song, K. C.; Dávila-Contreras, E. M.; Qi, Y.; Lee, J.; Monje-Galvan, V.; … Im, W. CHARMM-GUI *Membrane Builder* toward Realistic Biological Membrane Simulations. *J. Comput. Chem.* **2014**, *35*, 1997–2004.

(56) Li, M.; Binda, C.; Mattevi, A.; Edmondson, D. E. Functional Role of the "aromatic Cage" in Human Monoamine Oxidase B: Structures and Catalytic Properties of Tyr435 Mutant Proteins. *Biochemistry* **2006**, *45*, 4775–4784.

(57) Edmondson, D. E.; Binda, C.; Wang, J.; Upadhyay, A. K.; Mattevi, A. Molecular and Mechanistic Properties of the Membrane-Bound Mitochondrial Monoamine Oxidases. *Biochemistry* **2009**, *48*, 4220–4230.

(58) Søndergaard, C. R.; Olsson, M. H. M.; Rostkowski, M.; Jensen, J. H. Improved Treatment of Ligands and Coupling Effects in Empirical Calculation and Rationalization of P K a Values. *J. Chem. Theory Comput.* **2011**, *7*, 2284–2295.

(59) Chen, V. B.; Arendall, W. B.; Headd, J. J.; Keedy, D. A.; Immormino, R. M.; Kapral, G. J.; Murray, L. W.; Richardson, J. S.; Richardson, D. C. *MolProbity* : All-Atom Structure Validation for Macromolecular Crystallography. *Acta Crystallogr. Sect. D Biol. Crystallogr.* **2010**, *66*, 12–21.

(60) Best, R. B.; Zhu, X.; Shim, J.; Lopes, P. E. M.; Mittal, J.; Feig, M.; MacKerell, A. D. Optimization of the Additive CHARMM All-Atom Protein Force Field Targeting Improved Sampling of the Backbone Φ, ψ and Side-Chain χ1and χ2Dihedral Angles. *J. Chem. Theory Comput.* **2012**, *8*, 3257–3273.

(61) Klauda, J. B.; Venable, R. M.; Freites, J. A.; O'Connor, J. W.; Tobias, D. J.; Mondragon-Ramirez, C.; Vorobyov, I.; MacKerell, A. D.; Pastor, R. W. Update of the CHARMM All-Atom Additive Force Field for Lipids: Validation on Six Lipid Types. *J. Phys. Chem. B* **2010**, *114*, 7830–7843.

(62) Darden, T.; York, D.; Pedersen, L. Particle Mesh Ewald: An *N* ·log(*N*) Method for Ewald Sums in Large Systems. *J. Chem. Phys.* **1993**, *98*, 10089–10092.

(63) Roe, D. R.; Cheatham, T. E. PTRAJ and CPPTRAJ: Software for Processing and Analysis of Molecular Dynamics Trajectory Data. *J. Chem. Theory Comput.* **2013**, *9*, 3084–3095.

(64) Allen, W. J.; Lemkul, J. A.; Bevan, D. R. GridMAT-MD: A Grid-Based Membrane Analysis Tool for Use with Molecular Dynamics. *J. Comput. Chem.* **2009**, *30*, 1952–1958.